











Matter distribution of  $^{12-20,22}\text{C}$  isotopes

M. Mouadil <sup>1</sup>, A. Khouaja,<sup>1,\*</sup> O. Jdair <sup>2</sup>, Y. Elabssaoui <sup>1</sup>, M. L. Bouhssa <sup>3</sup>, H. Badane <sup>1</sup>, I. Mhali <sup>1</sup>, Z. Sobhy <sup>1</sup>,  
L. Hasbi <sup>1</sup>, B. Elouardi <sup>1</sup>, J. Inchaouh <sup>1</sup> and A. Morsad<sup>1</sup>

<sup>1</sup>Department of Physics, LPMC-ERSA, Faculty of Sciences Ben M'Sik, University of Hassan II, B.P 7955, 20800 Casablanca, Morocco

<sup>2</sup>Department of Physics, Polydisciplinary Faculty, Abdelmalek Essaadi University, B.P 745, 92004 Larache, Morocco

<sup>3</sup>Department of Physics, LPNAMME-GPTN, Faculty of Sciences, Chouaib Doukkali University, B.P 20, 24000 El Jadida, Morocco



(Received 30 October 2023; revised 24 November 2023; accepted 16 April 2024; published 31 May 2024)

The matter distribution is systematically studied for neutron-rich carbon isotopes with  $N = 6-16$  from the available measured reaction cross sections with  $^{12}\text{C}$  reaction target, using the finite-range Glauber model with Coulomb correction. We have first studied the energy dependence of the  $^{12}\text{C}-^{12}\text{C}$  reaction cross sections in a wide range of incident energies from 30–950 MeV/nucleon. A good agreement with the experimental data measured at low and high incident energy is obtained by considering the nuclear density distribution of two Fermi (2pF) parameters, where the two optimized parameters are the size parameter  $r_{2pF}$  and the diffusivity parameter  $a_{2pF}$ . We have therefore extracted the necessary parameters of the proton, neutron, and matter distributions for the whole range of  $^{12-20,22}\text{C}$  isotopes. With a set of calculations of four freely adjustable parameters (proton:  $r_{2pF,p}$ ,  $a_{2pF,p}$ ) and (neutron:  $r_{2pF,n}$ ,  $a_{2pF,n}$ ), we present for the first time an accurate determination of the neutron radii together with the proton radii, which are in excellent agreement with the charge radii directly extracted from the measured charge-changing cross sections. The evolution of the central density and diffuseness is studied as a function of the number of neutrons and shows the persistence of the  $N = 8$  shell closure for  $^{14}\text{C}$ . However, an anomalous halo structure is studied for the  $^{16,19,22}\text{C}$  isotopes, where the effect of proton-neutron nuclear interaction could be manifested by the decrease of the central density with large expansion at large distance, leading to a sharp increase of the radii with respect to the neighboring nuclei.

DOI: [10.1103/PhysRevC.109.054330](https://doi.org/10.1103/PhysRevC.109.054330)

## I. INTRODUCTION

The new radioactive nuclear beam facilities have provided excellent opportunities to study the structure of short-lived neutron-rich exotic nuclei [1], with the aim of extracting the necessary information about the nuclear matter distribution and nuclear size. Many experimental observables became accessible, including various inclusive cross sections, such as reaction or interaction cross sections, nucleon-removal cross sections, Coulomb breakup cross sections, and momentum distributions of a produced fragment [2,3]. These quantities allow us to reveal the anomalous structure, in particular the halo and skin when approaching the neutron drip line [2]. The neutron skin describes an excess of neutrons at the nuclear surface, whereas in the neutron halo the valence neutron can tunnel into the classical forbidden region due to its weak binding energy, forming the spatially extended wave function beyond the nuclear core potential. The first indication of halo nuclei was observed from the large matter root-mean-square of the  $^{11}\text{Li}$  radius ( $R_m = 3.27 \pm 0.24$  fm), derived from the interaction cross section at an incident energy of 790 MeV/nucleon [4]. The same indication described as an extended low-density distribution of valence neutrons surrounding a compact nuclear core is also observed in the elastic

scattering of protons from the helium isotopes of  $^6\text{He}$  and  $^8\text{He}$  at energies close to 700 MeV/nucleon. These nuclei are therefore observed to have root-mean-square radii of  $R_m = 2.30 \pm 0.07$  fm and  $R_m = 2.45 \pm 0.07$  fm, and a thickness of  $R_n - R_p = 0.61 \pm 0.21$  fm and  $R_n - R_p = 1.12 \pm 0.17$  fm, respectively [5–7]. Since then, many halo and skin nuclei have been discovered, and their unusual structure is discussed in detail by the authors of Refs. [8–10].

Recently, the structure of carbon isotopes has attracted much attention since most of them, such as  $^{15,16,19,22}\text{C}$ , have been suggested to have a halo structure based on some theoretical and experimental works [3,11–17]. The structure of  $^{22}\text{C}$  has been studied with a subshell closure of  $N = 16$ , which is proposed as a candidate for a new magic number [18]. In the framework of the three-body model the authors of Ref. [11] assumed that the  $^{22}\text{C}$  has a Borromean character (core plus two neutron halo), where neither the  $^{20}\text{C}$ -n nor the n-n subsystems are bound. This anomalous structure was experimentally demonstrated in the work of Tanaka *et al.* [13] by measuring a large reaction cross section ( $\sigma_R = 1.338 \pm 0.274$  barn) on a proton target at 40 MeV/nucleon, which is associated with a relatively large uncertainty of the radius-mean-squared matter  $R_m = 5.4 \pm 0.9$  fm. In the recent work of Togano *et al.* [12], the interaction cross section of  $^{22}\text{C}$  on a carbon target is observed to be larger than that of its neighboring isotopes  $^{19,20}\text{C}$  and is measured to be  $\sigma_R = 1.280 \pm 0.023$  barn at an incident energy of 235 MeV/nucleon. And the rms matter

\*abdenbikhouaja@gmail.com

radius ( $R_m = 3.44 \pm 0.04$  fm) derived from the four-body Glauber model analysis, was in good agreement with the theoretical predictions [11] based on  $^{22}\text{C}$  three-body model wave functions, supporting a two neutron halo structure of  $^{22}\text{C}$ . Further evidence for the anomalous nature of this nucleus is summarized in Ref. [14], where a narrow momentum distribution is observed from the measured two-neutron removal cross section of  $^{22}\text{C}$  at energy (around 240 MeV/nucleon).

In addition, a neutron halo structure has been suggested for  $^{15}\text{C}$  by measuring the intermediate energy reaction cross section as well as the longitudinal momentum distribution of the  $^{14}\text{C}$  fragment from the breakup of  $^{15}\text{C}$  at 83 MeV/nucleon [3,15]. However, there is no evidence for such a halo structure from the interaction cross section measurements at relativistic energy [19]. Recently, Rashdan *et al.* [16] studied the exotic structure of  $^{15}\text{C}$  with  $^{12}\text{C}$  and  $^{27}\text{Al}$  reaction targets as a one-neutron halo nucleus by calculating the reaction cross section at the intermediate energy (20–300 MeV/nucleon) of  $^{15,16}\text{C} + ^{12}\text{C}$  using the microscopic complex optical potential. Zheng *et al.* [20] have measured the reaction cross sections for  $^{12,16}\text{C} + ^{12}\text{C}$  at 83 MeV/nucleon; the results showed a large enhancement of the  $^{16}\text{C}$  reaction cross section. These data were analyzed in the framework of the finite-range Glauber model and showed a large extension of the neutron density distribution, far from the center of the nucleus, suggesting the formation of a neutron halo in the  $^{16}\text{C}$  nucleus. Another anomalous structure has been investigated in  $^{19}\text{C}$  by Kanungo *et al.* [17], where a halo structure is proposed when the proton distribution of isotopes  $^{12-19}\text{C}$  radii is derived from the measurements of charge-changing cross sections with a carbon target at 900 MeV/nucleon.

The density distribution of unstable nuclei is not easily determined by the elastic scattering experiment used for stable nuclei: the short-lived nature of unstable nuclei does not allow them to be shaped into a target. The measurement of the reaction cross section from elastic scattering in inverse kinematics is a powerful tool to extract the density distribution of unstable nuclei using the Glauber model. At high energies, this model is well established for reproducing the measured reaction cross section. However, at low and intermediate energies, the standard (zero range) Glauber model underestimates the cross section [19]. To overcome this discrepancy, some modifications such as the profile function (finite range) and the Coulomb repulsion effect on the incident particle trajectory have been taken into account.

In the present work, we used the finite-range modified Coulomb Glauber model for large-scale investigation of the matter distribution of  $^{12-20,22}\text{C}$  isotopes. As one of the necessary required input data, we used the two-parameter Fermi functional form (2pf density) for the nuclear density distribution. We also used the analytical slope-range parametrization and the total nucleon-nucleon cross section. From a set of available experimental data measured with the  $^{12}\text{C}$  reaction target, we theoretically reproduced the energy dependence of the reaction cross sections, using the best fit of  $\chi^2$ , in a wide range of incident interaction energies from 30–950 MeV/nucleon. We then extracted the two parameters of diffuseness  $a_{2pF}$  and reduced radius  $r_{2pF}$  from the two parameters of Fermi density, and then calculated the

root-mean-square (rms) radii of protons, neutrons, and matter for the wide range of  $^{12-20,22}\text{C}$  isotopes.

In such an optimal context, this paper is organized as follows. In Sec. II, we presented the formalism of the finite-range modified Coulomb Glauber model for the calculation of the reaction cross section. We first studied the energy dependence of the  $^{12}\text{C} - ^{12}\text{C}$  reaction cross section by assuming the 2pF-type density form. With the two optimized parameters,  $a_{2pF}$  and  $r_{2pF}$ , we were able to determine well the rms radii of protons, neutrons, and  $^{12}\text{C}$  matter in comparison with the available calculated ones when assuming HO and Gaussian type densities. As described in Sec. III, we have therefore studied the matter distribution (density and radii of protons, neutrons, and matter). In the end we conclude this paper with rich information on the ability of the modified Glauber model to reproduce well the matter distribution of neutron-rich exotic nuclei and discussed the skin and halo structure from the density.

## II. THEORETICAL FORMALISM

Theoretically, the reaction cross section is intensively studied to predict the matter distribution and transparency of nuclei. Within the standard Glauber model [21], under the optical limit approximation [22], the nucleus-nucleus reaction cross section is well reproduced at high incident energy, and is smoothly corrected for lower energy, where the effect of Coulomb repulsion between projectile and target is more significant [23,24]. The reaction cross section is then expressed,

$$\sigma_R = 2\pi \left( 1 - \frac{V_c}{E_{c.m.}} \right) \int b db [1 - T(b)], \quad (1)$$

where  $V_c$  and  $E_{c.m.}$  are the Coulomb barrier and the incident energy at the center of mass, respectively.  $T(b)$  is the transparency function with a given incident parameter  $b$ . This function  $T(b)$  is defined as the probability of nonreactions or at least one nucleon-nucleon reaction occurring in the overlapping region of the projectile and the target. It is calculated by assuming a single nucleon-nucleon collision,

$$T(b) = \exp(-\sigma_{\text{tot}}^{\text{NN}} \chi(b)). \quad (2)$$

The total free nucleon-nucleon cross section  $\sigma_{\text{tot}}^{\text{NN}}$  is averaged over the experimental proton-proton,  $\sigma_{pp}$ , proton-neutron,  $\sigma_{pn}$ , and neutron-neutron cross sections,  $\sigma_{nn}$  and is then calculated using the expression [25,26]

$$\sigma_{\text{tot}}^{\text{NN}} = \frac{Z_P Z_T \sigma_{pp} + N_P N_T \sigma_{nn} + (N_P Z_T + Z_P N_T) \sigma_{np}}{A_P A_T} \quad (3)$$

where  $A_P$ ,  $A_T$ ,  $Z_P$ ,  $Z_T$ , and  $N_P$ ,  $N_T$  are the mass, charge and neutron numbers for the projectile and the target, subscripted  $P$  and  $T$ , respectively.  $\chi(b)$  is the nuclear phase shift which, in the optical limit approximation, can be expressed over the overlapping integrated densities as follows [26],

$$\chi(b) = \iint d^2 b_1 \iint d^2 b_2 f(|b_1 - b_2|) \rho_z^P(b_1) \rho_z^T(|b_2 - b|), \quad (4)$$

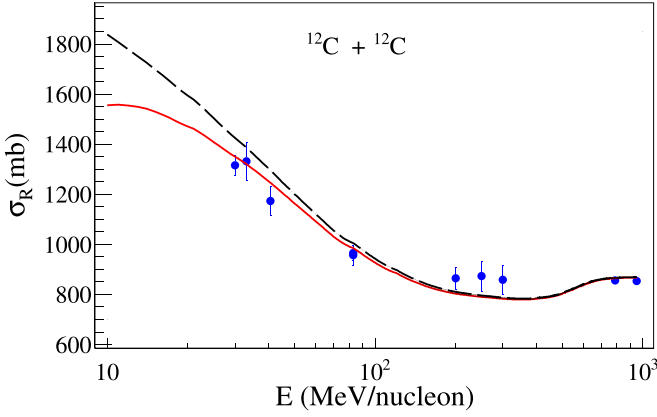


FIG. 1. Energy dependence of the calculated  $^{12}\text{C} + ^{12}\text{C}$  reaction cross sections with the Coulomb-modified Glauber model (red line) and the standard Glauber model (black dashed line) in comparison with the available experimental data (blue solid circles) from Refs. [20,23,27,28].

where  $\rho_z^{P,T}(b)$  is the thickness density, expressed along the  $z$  coordinate, the beam direction and the impact parameter  $b$  as,

$$\rho_z^{P,T}(b) = \int_{-\infty}^{+\infty} dz \rho_{P,T}(\sqrt{b^2 + z^2}) \quad (5)$$

and  $f(|b_1 - b_2|)$  is the profile function that makes the Glauber model work reasonably well from the low- to the high-energy range [25]. Within the finite range of this formalism, this function is usually parameterized in the Gaussian form [22]:

$$f(b) = \frac{1 - i\alpha}{4\pi \varepsilon_{\text{NN}}^2} \exp\left(-\frac{b^2}{2\varepsilon_{\text{NN}}^2}\right) \quad (6)$$

where  $\varepsilon_{\text{NN}}$  is the range parameter and  $i\alpha$  is the ratio of the real to the imaginary part of the forward scattering amplitude, which we assumed to be zero in the calculation of  $\sigma_R$  in the optical limit approximation [20,29]. The values of the range parameter  $\varepsilon_{\text{NN}}$  are difficult to find accurately, especially at lower energies where the matter distribution is very sensitive to a large tail such as halo and skin. In the literature, we found different values of  $\varepsilon_{\text{pp}}$  and  $\varepsilon_{\text{pn}}$  [30], which could be the source of large uncertainties in the calculation of the reaction cross section [22]. However, the range parameter is assumed to depend smoothly on the incident energy and to be the same for all combinations of neutrons and protons. We then used the new range parameter parametrization of Zheng [20], obtained by fitting the  $^{12}\text{C} + ^{12}\text{C}$  reaction cross section from 30 MeV/nucleon to 1 GeV/nucleon, as

$$\varepsilon_{\text{NN}} = 0.996 \exp\left(-\frac{E}{106.679}\right) + 0.089. \quad (7)$$

As shown in Fig. 1, we have numerically calculated the total reaction cross sections for  $^{12}\text{C} + ^{12}\text{C}$  collisions using Eqs. (1)–(7). For convenience, we have also plotted the calculations from the standard Glauber model (black dashed line), which is overestimated by 2–7 % from intermediate to low energies according to the Coulomb-modified model (red line). We see that the results of our calculations agree well, both at high and low energies, are in good agreement

with the available experimental data from Refs. [20,23,27,28]. The main parameters in these calculations are the densities of the projectile and target nuclei. The proton-proton  $\sigma_{\text{pp}}$  and proton-neutron  $\sigma_{\text{pn}}$  cross sections are obtained by smooth interpolation of the experimental values from Ref. [31] using the nijisiki subroutine, for the entire incident energy range from 10–950 MeV/nucleon. Since the reaction cross section is known to be very sensitive to the surface part of the density distribution, namely the tail region [32], the choice of the density profile must be carefully considered. We then used the Fermi 2pF type density, which is normally used to study the medium and heavy nuclei. We have extended the use of this type of density to the light neutron-rich carbon isotopes, where the valence neutrons of the surface region are the main source of skin and halo structures. The density is expressed in the form of [33,34],

$$\rho_{k,2pf}(r) = \frac{\rho_{0,k}}{1 + \exp\left(\frac{r - R_{k,2pf}}{a_{k,2pf}}\right)}. \quad (8)$$

The subscript  $k = Z(N)$  indicates the number of protons and neutrons, respectively.  $\rho_{0,k}$  is the central density, determined by the normalisation condition as

$$\rho_{0,k} = \frac{3k}{4\pi R_{k,2pf}^3} \left(1 + \frac{\pi^2 a_{k,2pf}^2}{R_{k,2pf}^2}\right)^{-1}, \quad (9)$$

where  $R_{k,2pf} = r_{2pf} \cdot Z^{1/3}$  (or  $N^{1/3}$ ) is the charge radius and  $a_{k,2pf}$  is the surface diffusivity. By integrating this density using these two essential parameters, which are optimized (extracted) from the measured reaction cross section, we then express, under normalization, the rms radii of the neutron and proton, respectively, as:

$$\langle r^2 \rangle_n = \frac{3}{5} R_{n,2pf}^2 \left[1 + \frac{7\pi^2 a_{n,2pf}^2}{3R_{n,2pf}^2}\right] \quad (10)$$

$$\langle r^2 \rangle_p = \frac{3}{5} R_{p,2pf}^2 \left[1 + \frac{7\pi^2 a_{p,2pf}^2}{3R_{p,2pf}^2}\right] \quad (11)$$

and the charge radius, which can be derived from that of the proton,

$$\langle r^2 \rangle_{\text{ch}} = \langle r^2 \rangle_p + 0.64 \text{ fm}^2. \quad (12)$$

The rms radius of matter is finally expressed as

$$\langle r^2 \rangle_m = (Z/A) \langle r^2 \rangle_p + (N/A) \langle r^2 \rangle_n. \quad (13)$$

For convenience, we have defined the rms sizes below as  $R_p = \langle r^2 \rangle_p^{1/2}$  for protons,  $R_n = \langle r^2 \rangle_n^{1/2}$  for neutrons, and  $R_m = \langle r^2 \rangle_m^{1/2}$  for matter.

We have used the best fit between the experimental and the calculated reaction cross sections according to the formula,

$$\chi^2 = \sum_n \frac{[\sigma_R(\text{expt}) - \sigma_R(\text{theo})]^2}{d\sigma_R(\text{expt})} \quad (14)$$

where  $\sigma_R(\text{expt})$  and  $d\sigma_R(\text{expt})$  are the experimental reaction cross section and its reported uncertainty, and  $\sigma_R(\text{theo})$  is the calculated reaction cross section. The resulting best fit is made as a function of the dependent incident energy  $E$  from low (10 MeV/nucleon) to high energy (950 MeV/nucleon).

TABLE I. Parameters, given in fm, of the 2pF density distributions and the proton, neutron, and matter rms radii of the  $^{12-20,22}\text{C}$  isotopes. The results are obtained in the case of 2P set calculations.

Nucleus	$r_{2pf,p}$	$a_{2pf,p}$	$r_{2pf,n}$	$a_{2pf,n}$	$R_p$	$R_n$	$R_m$
12	$1.114 \pm 0.017$	$0.453 \pm 0.004$	$1.114 \pm 0.017$	$0.453 \pm 0.004$	$2.306 \pm 0.015$	$2.306 \pm 0.015$	$2.306 \pm 0.021$
13	$1.071 \pm 0.010$	$0.429 \pm 0.004$	$1.071 \pm 0.010$	$0.429 \pm 0.004$	$2.207 \pm 0.012$	$2.267 \pm 0.015$	$2.242 \pm 0.019$
14	$1.065 \pm 0.014$	$0.430 \pm 0.004$	$1.065 \pm 0.014$	$0.430 \pm 0.004$	$2.198 \pm 0.013$	$2.299 \pm 0.013$	$2.259 \pm 0.018$
15	$1.075 \pm 0.008$	$0.488 \pm 0.012$	$1.075 \pm 0.008$	$0.488 \pm 0.012$	$2.360 \pm 0.020$	$2.512 \pm 0.027$	$2.450 \pm 0.033$
16	$1.092 \pm 0.011$	$0.539 \pm 0.008$	$1.092 \pm 0.011$	$0.539 \pm 0.008$	$2.520 \pm 0.010$	$2.718 \pm 0.014$	$2.651 \pm 0.017$
17	$1.096 \pm 0.011$	$0.545 \pm 0.004$	$1.096 \pm 0.011$	$0.545 \pm 0.004$	$2.537 \pm 0.007$	$2.767 \pm 0.025$	$2.677 \pm 0.026$
18	$1.087 \pm 0.013$	$0.557 \pm 0.007$	$1.087 \pm 0.013$	$0.557 \pm 0.007$	$2.585 \pm 0.010$	$2.851 \pm 0.026$	$2.780 \pm 0.030$
19	$1.168 \pm 0.020$	$0.619 \pm 0.010$	$1.168 \pm 0.020$	$0.619 \pm 0.010$	$2.817 \pm 0.025$	$3.126 \pm 0.067$	$3.049 \pm 0.071$
20	$1.164 \pm 0.031$	$0.576 \pm 0.024$	$1.164 \pm 0.031$	$0.576 \pm 0.024$	$2.692 \pm 0.034$	$3.043 \pm 0.073$	$2.963 \pm 0.080$
22	$1.197 \pm 0.040$	$0.665 \pm 0.020$	$1.197 \pm 0.040$	$0.665 \pm 0.020$	$2.986 \pm 0.050$	$3.408 \pm 0.077$	$3.298 \pm 0.091$

We optimized the dependence of the experimental and calculated  $^{12}\text{C} + ^{12}\text{C}$  reaction cross sections with parameters  $r_{2pf} = 1.117 \pm 0.020$  fm and  $a_{2pf} = 0.453 \pm 0.005$  fm, which are considered to be the same for both proton and neutron densities, since the  $^{12}\text{C}$  nucleus has the same number of protons and neutrons. We then calculated the corresponding effective radii:  $R_p = 2.305 \pm 0.020$  fm,  $R_n = 2.305 \pm 0.020$  fm, and  $R_m = 2.305 \pm 0.020$  fm. We therefore found that our calculated results compare well with the majority of previous theoretical and experimental work that assumed a density distribution for  $^{12}\text{C}$  that is either Gaussian or Harmonic oscillator (HO) [35–40]. Furthermore, in the framework of Fermi model, Farid *et al.* [41] calculated the rms of matter  $R_m = 2.298$  fm for  $^{12}\text{C}$  from the Fermi parameters,  $a_{2pf} = 0.425$  fm and  $r_{2pf} = 1.185$  fm. Using the double-folding formalism for the  $\alpha$ -nucleus optical potential, Khoa [42] obtained the ground-state density distribution parameters for  $^{12}\text{C}$ ,  $a_{2pf} = 0.425$  fm and  $r_{2pf} = 1.218$  fm, with the corresponding rms radius  $R_m = 2.332$  fm. Otherwise, under the optical Glauber model, Rashdan [43] reproduced the rms radius  $R_m = 2.450$  fm from the adjusted reduced radius,  $r_{2pf} = 1.211$  fm, and diffuseness,  $a_{2pf} = 0.475$  fm, when fitting the experimental data of the  $^{12}\text{C} + ^{12}\text{C}$  reaction cross section as a function of incident energy between 100 and 1000 MeV/nucleon. We then see that the rms radius value obtained from Ref. [43] is smaller than our calculated rms radius; this shows how important the reliable information on nuclear densities and radii is when studying the energy dependence of the reaction cross section. However, the configuration of the medium as a function of the charge distribution in the center and the diffusivity in the surface is likely to be more influential in the structure of both stable and exotic nuclei.

Experimentally, the charge radius of  $^{12}\text{C}$  is simultaneously evaluated to be  $\langle r^2 \rangle_{\text{ch}}^{1/2} = 2.470 \pm 0.02$  fm by the two experimental methods including electron scattering and muonic atom x rays [44]. Within the framework of the relativistic mean field (RMF) and its extension based on the field theory motivated effective Lagrangian approach, known as E-RMF, Shuckla *et al.* [45] calculated the charge radius  $R_{\text{ch}} = 2.466$  fm with RMF and  $R_{\text{ch}} = 2.497$  fm with E-RMF formalisms. Under the assumption that the considered nucleus could be treated as a nucleus plus one or two valence neutrons, a simple theoretical model was used by Abu-Ibrahim *et al.* [46]

to calculate the nuclear radii of  $^{12}\text{C}$  with  $R_p = 2.330$  fm,  $R_n = 2.300$  fm, and  $R_m = 2.310$  fm; which are in good agreement with our calculated results.

Consequently, the density parameters,  $r_{2pF}$  and  $a_{2pF}$ , are well tuned for the  $^{12}\text{C}$  target. We have further investigated the energy dependence of the reaction cross sections for the  $^{12-20,22}\text{C} - ^{12}\text{C}$  systems.

### III. RESULTS and DISCUSSION

We have calculated the reaction cross sections of  $^{12-20,22}\text{C} - ^{12}\text{C}$  reacting systems, depending on the available experimental data from Refs. [3,12,15,20,23,27,28,47–50] over a wide range of incident energies (30–950 MeV/nucleon). We performed the best-fit procedure using Eq. (14), under two sets of calculations considered. We treated the reacting projectile density as a problem of two adjustable parameters (denoted 2P) with,  $r_{2pF,p} = r_{2pF,n} = r_{2pF}$  and  $a_{2pF,p} = a_{2pF,n} = a_{2pF}$ . And we also considered the reacting projectile density as a problem of four free parameters (denoted 4P) with,  $r_{2pF,p} \neq r_{2pF,n}$  and  $a_{2pF,p} \neq a_{2pF,n}$ . For some nuclei, especially the short-lived ones, the number of available measured reaction cross sections does not allow us to firmly divide between the optimized parameters of the densities. To overcome this limitation, we started the calculations with initial values of  $r_{2pF,p}$  and  $r_{2pF,n}$  from Refs. [51,52] and set  $a_{2pF,p}$  and  $a_{2pF,n}$  up to 0.2 fm. Step by step of 0.1 fm, we obtained the centroid of optimized values of 2pF densities as listed in Tables I and II, respectively, for the two sets of calculations of 2P and 4P. We derived, as tabulated together, using Eqs. (10), (11), (13) the reliable information about the nuclear radii, called root-mean-square (rms) radii,  $R_p$  for proton,  $R_n$  for neutron, and  $R_m$  for matter; which are considered as the main objective of the present study.

#### A. RMS radii of protons, neutrons, and matter

For  $N = 6-16$  neutron-rich carbon isotopes, Abu-Ibrahim *et al.* [46], when studying the reaction cross sections, showed a rapid change in the radii of  $^{19}\text{C}$  and  $^{22}\text{C}$ , which were estimated to be one- and two-neutron halos, respectively. They pointed out that the major contribution to the reaction cross section comes from the surface region, especially at lower

TABLE II. Parameters, given in fm, of the 2pF density distributions and the proton, neutron and matter rms radii of the  $^{12-20,22}\text{C}$  isotopes. The results are obtained in the case of 4P set calculations.

Nucleus	$r_{2pf,p}$	$a_{2pf,p}$	$r_{2pf,n}$	$a_{2pf,n}$	$R_p$	$R_n$	$R_m$
12	$1.117 \pm 0.020$	$0.453 \pm 0.005$	$1.117 \pm 0.020$	$0.453 \pm 0.005$	$2.305 \pm 0.020$	$2.305 \pm 0.020$	$2.305 \pm 0.03$
13	$1.146 \pm 0.015$	$0.424 \pm 0.004$	$1.137 \pm 0.014$	$0.389 \pm 0.009$	$2.272 \pm 0.017$	$2.239 \pm 0.010$	$2.250 \pm 0.020$
14	$1.161 \pm 0.019$	$0.433 \pm 0.007$	$1.134 \pm 0.016$	$0.377 \pm 0.011$	$2.307 \pm 0.031$	$2.250 \pm 0.030$	$2.278 \pm 0.043$
15	$1.117 \pm 0.008$	$0.468 \pm 0.012$	$1.128 \pm 0.015$	$0.475 \pm 0.002$	$2.363 \pm 0.023$	$2.543 \pm 0.019$	$2.464 \pm 0.030$
16	$1.127 \pm 0.010$	$0.488 \pm 0.022$	$1.163 \pm 0.021$	$0.539 \pm 0.004$	$2.404 \pm 0.055$	$2.783 \pm 0.036$	$2.649 \pm 0.066$
17	$1.115 \pm 0.007$	$0.499 \pm 0.022$	$1.145 \pm 0.019$	$0.543 \pm 0.003$	$2.413 \pm 0.056$	$2.832 \pm 0.031$	$2.692 \pm 0.064$
18	$1.121 \pm 0.007$	$0.476 \pm 0.030$	$1.179 \pm 0.026$	$0.561 \pm 0.002$	$2.376 \pm 0.078$	$2.950 \pm 0.033$	$2.782 \pm 0.084$
19	$1.176 \pm 0.020$	$0.482 \pm 0.067$	$1.267 \pm 0.035$	$0.612 \pm 0.014$	$2.438 \pm 0.124$	$3.264 \pm 0.058$	$3.021 \pm 0.137$
20	$1.116 \pm 0.022$	$0.473 \pm 0.103$	$1.206 \pm 0.040$	$0.594 \pm 0.011$	$2.369 \pm 0.156$	$3.153 \pm 0.082$	$2.938 \pm 0.175$
22	$1.220 \pm 0.056$	$0.466 \pm 0.090$	$1.357 \pm 0.050$	$0.642 \pm 0.038$	$2.452 \pm 0.091$	$3.565 \pm 0.084$	$3.296 \pm 0.123$

incident energies. The same behavior was shown by Kanungo *et al.* [17] from the charge-changing cross section measurements. A thick neutron surface is shown in  $^{15}\text{C}$  and  $^{19}\text{C}$ , previously observed with large halo radii. They determined for the first time the point-proton distributions and the skin effect as a function of the neutron surface distribution. This structural effect was first discovered by Yamaguchi *et al.* [53], where the density distribution of protons in the nuclei was found to be tightly bounded. In Fig. 2, we have plotted our calculated rms point-proton and point-neutron radii against those available in Refs. [17,27,35,40,46,47,54], as a function of  $N = 6-16$ . The closed blue and black circles are the results of our 2P and 4P set calculations, respectively; the connecting lines are shown to show their evolution. In the case of the 4P set where the number of data is insufficient (more than four measured reaction cross sections), the calculated rms radii are presented with a larger uncertainty (error bar), but the ratio between the two matter radii from 2P and 4P is observed to be close to unity, whereas the 2P set calculations greatly overestimate the rms point-proton radii. As shown in this figure and within the error bar, we see that the results of the 4P set calculations are more in agreement with the results

of the point-proton and point-neutron distributions determined experimentally from the charge-changing (exchange) cross sections [17,27,55]. The behavior of the rms radii increases with neutron number, the same as observed in the calculations of Abu-Ibrahim *et al.* [46] and Suhel *et al.* [40], where the harmonic oscillator density is considered for the reacting projectile. We have pointed out here the usefulness of the 2pF density to study the matter distribution in the surface region, where the neutron distribution may influence the point charge distribution. Therefore, in Fig. 3, we defined the neutron skin thickness as the difference of the point-neutron ( $R_n$ ) and point-proton ( $R_p$ ) radii from the 4P calculation set. The black closed circles are, respectively, our calculation results, which compare well with the determined experimental results (red closed circles) from Ref. [17]. We then see a gradual increase in the neutron skin thickness, which evolves from 0–1.1 fm as the neutron-proton asymmetry increases. This nuclear surface effect is associated with the large Fermi level difference between neutrons and protons as the nuclei become highly neutron rich [17].

The matter radii of  $^{12-20,22}\text{C}$  are shown in Fig. 4 to be in good agreement with the results of Refs. [17,27], although

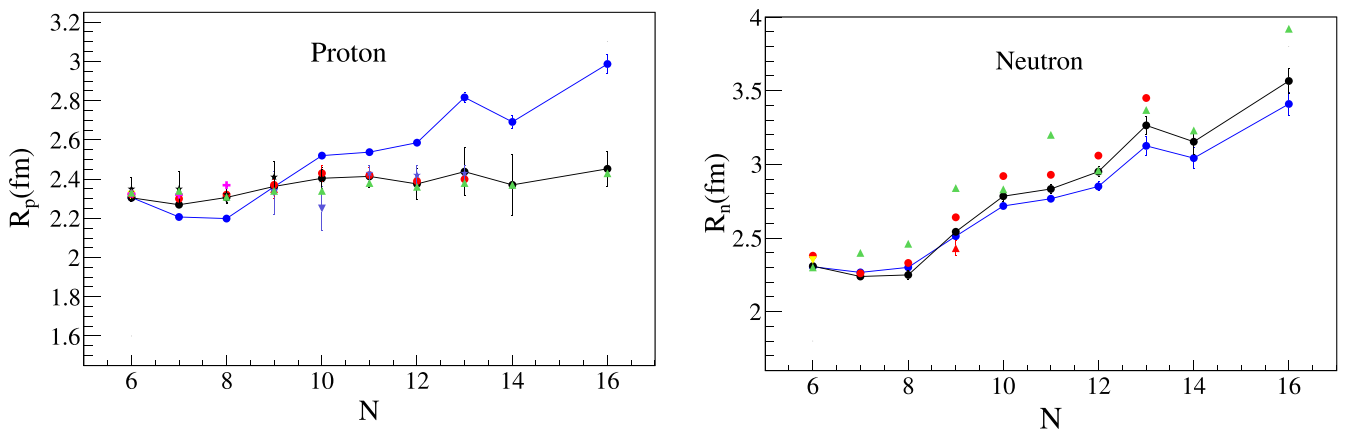


FIG. 2. The results of point-proton (left) and point-neutron (right) rms radii for  $^{12-20,22}\text{C}$  isotopes obtained from the two sets of calculations 2P (blue line and closed circles) and 4P (black line and closed circles). The results are compared with the available data from the literature: green closed up triangle for  $^{12-20,22}\text{C}$  [46], red closed circles for  $^{12-19}\text{C}$  [17], red closed up triangle, for  $^{15}\text{C}$  [47], yellow closed down triangle for  $^{12}\text{C}$  [35], black star for  $^{12-16}\text{C}$  [56], purple star for  $^{17,18,19}\text{C}$  [57], purple closed down triangle for  $^{15,16}\text{C}$  [53], and magenta full cross for  $^{12,13,14}\text{C}$  [58].

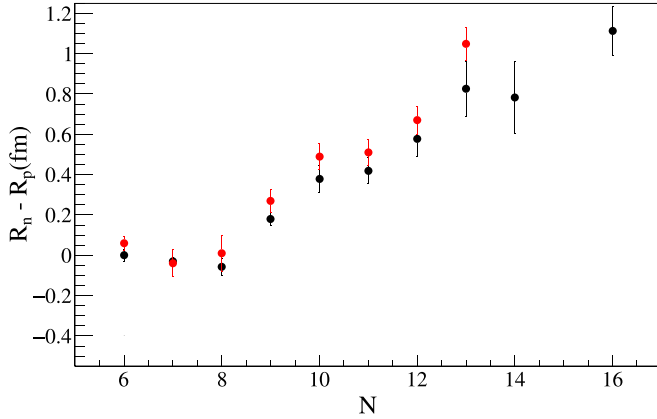


FIG. 3. The surface thickness, defined as the difference between the neutron and proton rms radii, is plotted as a function of the neutron number for the carbon isotopes of  $^{12-20,22}\text{C}$ . The black closed circles represent the results of the 4P set calculations compared to the data from Ref. [17], represented by the red closed circles.

less estimated than the results of Refs. [35,40,46,47,54]. We see a rapid change for  $^{16}\text{C}$ ,  $^{19}\text{C}$ , and  $^{22}\text{C}$  nuclei calculated with  $R_m = 2.649 \pm 0.066$  fm,  $3.021 \pm 0.137$  fm, and  $3.296 \pm 0.123$  fm, respectively, which are in good agreement with those extracted from measured reaction cross sections,  $R_m = 2.74 \pm 0.03$  fm,  $3.16 \pm 0.03$  fm [17],  $3.13 \pm 0.07$  fm [27], and  $3.44 \pm 0.08$  fm [12]. These nuclei have already been proposed to have a halo structure due to their large  $R_m$  radii and the dominance of the  $2S_{1/2}$  configuration of the valence neutrons calculated with empirical separation energies,  $S_{2n} = 5.468$  MeV ( $^{16}\text{C}$ ),  $S_n = 0.16$  MeV ( $^{19}\text{C}$ ) [59], and

$S_{2n} = 0.56$  MeV ( $^{22}\text{C}$ ) [12]. This suggestion could be deeply enriched if we consider the thickness of the extended valence neutrons as shown in Fig. 3 with 0.379 fm ( $^{16}\text{C}$ ), 0.826 fm ( $^{19}\text{C}$ ), and 1.133 fm ( $^{22}\text{C}$ ). Otherwise, from the increasing behavior of the skin thickness, we see that the  $^{14}\text{C}$  has less effect than the neighboring nuclei, which could be explained by the persistence of the  $N = 8$  shell closure. Such structural effects can be further observed from the density distribution when many more neutrons are added.

### B. Proton, neutron, and matter density distributions

Recently, Tanihata *et al.* [55], when studying the interaction of neutron-rich carbon isotopes with hydrogen, carbon, and nitrogen reaction targets, reported that the charge exchange cross sections increased much more with the carbon target than the others. The same observation was reported by Yamaguchi *et al.* [53] where the density distribution of protons in nuclei is tightly bound. However, we have plotted the point-proton, point-neutron, and matter density distributions as a function of the distance from the center of the nuclei, as shown in Fig. 5. We see a sensitivity of the point-charge (center) and point-neutron (surface) distributions when the density profile is plotted on linear (left side) and logarithmic (right side) scales.

As can be seen in Fig. 5, the proton density is manifested by a high central density, which decreases as the neutron number increases. This change is more pronounced in the center for the  $^{16}\text{C}$ ,  $^{19}\text{C}$ , and  $^{22}\text{C}$  nuclei, but it does not affect the surface part of the proton distribution, where the scattering at large distances is less important. This observation could explain the flatness of the proton rms radii seen in Fig. 2.

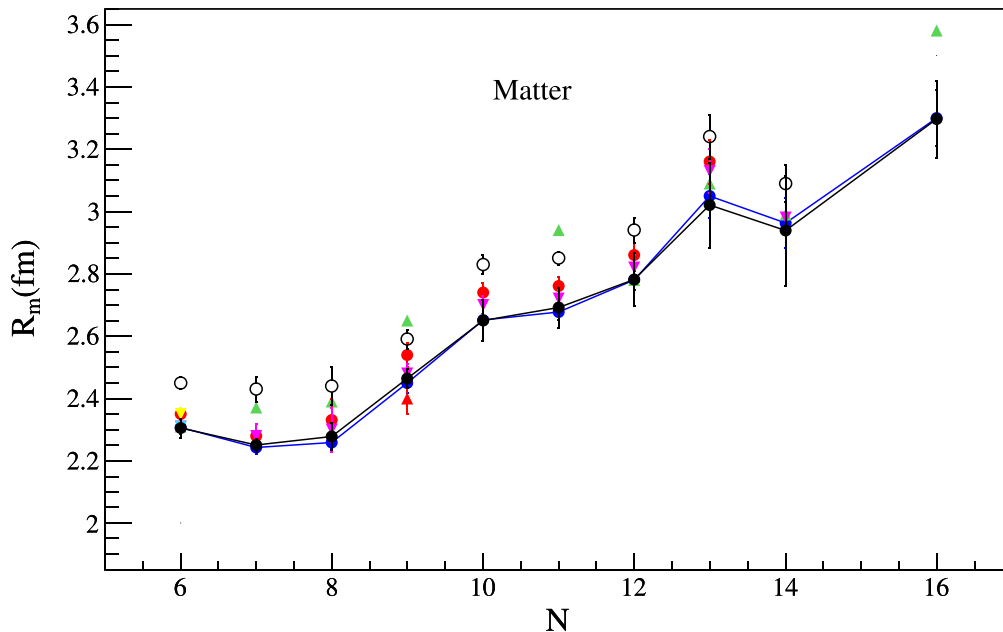


FIG. 4. The rms matter radii of  $^{12-20,22}\text{C}$  isotopes are compared with those extracted from the available experimental data of reaction cross sections: The results of Ref. [46] for  $^{12-20,22}\text{C}$  are shown with green up triangles,  $^{12-19}\text{C}$  [17] with closed red circles,  $^{15}\text{C}$  [47] with red closed up triangles,  $^{12}\text{C}$  [35] with yellow closed down triangles and sky blue down triangles from [54],  $^{12-20}\text{C}$  [40] with open black circles,  $^{12-20}\text{C}$  [27] with the magenta down triangles. The closed blue and black circles are our results with the calculation set 2P and 4P for  $^{12-20,22}\text{C}$ .

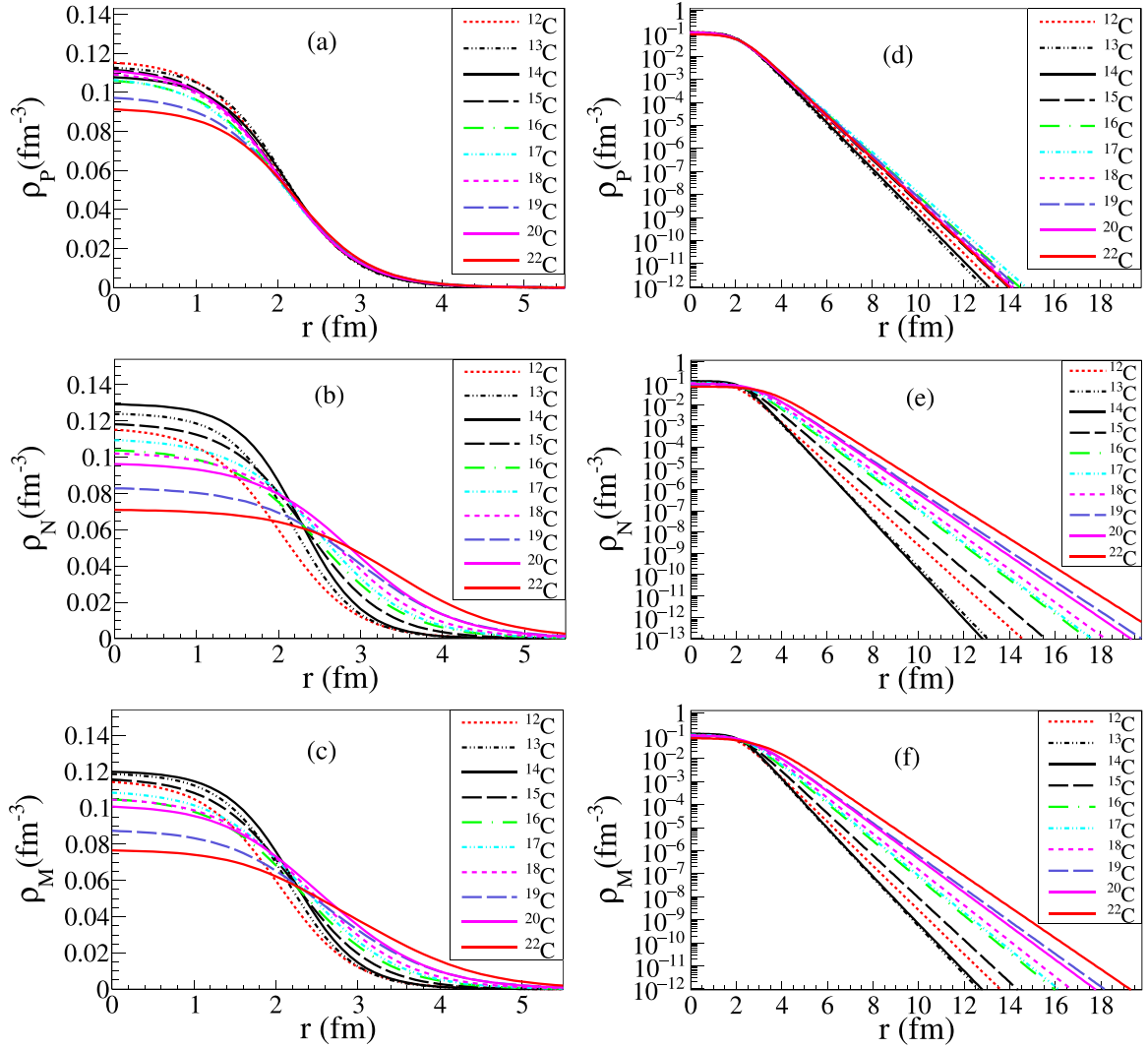


FIG. 5. The proton, neutron, and matter density distributions for the  $^{12-20,22}\text{C}$  isotopes. On the left side the central charge evolution is shown in linear scale, on the right side, the surface distribution is shown in logarithmic scale.

For the neutron density, the landscape is shown with a large spread (diffuseness) in the surface at large distances, as well as a more pronounced decrease in the central density as the number of neutrons increases. We see a smooth increase in the central density from  $^{12}\text{C}$  up to  $^{14}\text{C}$  with a reduced spread in the surface region, which could be explained by the persistence of  $N = 8$  magicity in  $^{14}\text{C}$ . Thereafter, the neutron distribution appears to be very sensitive to the proton-neutron asymmetry. We see a monotonically strong decrease in the central density coupled with a large diffuseness, leading to a large tail of nuclei as observed at large neutron rms radii (see Fig. 2).

The matter distribution is strongly influenced by the neutron distribution in the center as well as in the surface. There is clear evidence for the nuclei of  $^{16}\text{C}$ ,  $^{19}\text{C}$ , and  $^{22}\text{C}$  where the central density is less important than the neighboring nuclei and then the matter rms radii increase suddenly. This sudden increase could be explained by the dominance of the  $2S_{1/2}$  configuration of valence neutrons with low centrifugal barrier

[11,60]. Therefore, considering the weak separation energy, the large rms radii, the weakness of the central density and its large scattering at the larger distances, we can conclude that the  $^{16}\text{C}$ ,  $^{19}\text{C}$ , and  $^{22}\text{C}$  show an anomalous structure such as the neutron halo(s).

As a consequence, the 2pF-type density distribution seems to describe the proton and neutron distributions better than the other: HO and Gaussian density distributions since each has only one size parameter  $a_G$  and  $a_{HO}$ , respectively. The importance of this form of densities lies in the size parameter  $r_{2pF}$  and the diffuseness parameter  $a_{2pF}$ , which describe the surface region. According to the information treated in this work, the 2pF-type densities allowed us to explain the large values of the rms matter radius, in contrast to what is claimed in Ref. [40], where the HO densities can't predict whether the larger value of the rms matter radius of a neutron-rich nucleus near the drip line is due to the thicker neutron skin or to a halo structure. For loosely bound nuclei, the study of the density model is extended to the (nucleus + neutron) or (HO

plus Yukawa square function), which describes the asymptotic behavior of the wave function (long tail) for the neutron(s) halo, as has been done in several works [19,20,48,49].

#### IV. CONCLUSION

The matter distribution of  $^{12-20,22}\text{C}$  isotopes is studied using the finite-range Glauber model with Coulomb correction. The rms radii of protons, neutrons and matter are extracted from a set of available experimental data of reaction cross sections measured with a carbon target over a wide range of incident energies 30–950 MeV/nucleon. We have used the 2pF density to study the evolution of the matter distribution as a function of neutron number. Using the two parameters of diffuseness  $a_{2pF}$  and reduced radius  $r_{2pF}$ , we defined two sets of calculations (2P) :  $r_{2pF,p} = r_{2pF,n}$  and  $a_{2pF,p} = a_{2pF,n}$ ,

and (4P) :  $r_{2pF,p} \neq r_{2pF,n}$  and  $a_{2pF,p} \neq a_{2pF,n}$ . The 4P calculations showed an excellent agreement with the proton rms radii obtained directly from measured charge exchange cross sections, and then the matter rms radii evolved with the proton-neutron asymmetry parameter. The 2pF densities and rms radii of protons, neutrons, and matter of the  $^{12-20,22}\text{C}$  isotopes have been unambiguously determined for the first time. The central Coulomb barrier, as a function of the central charge distribution is shown to weaken with increasing number of neutrons, except for the  $^{14}\text{C}$  nucleus where the magic of  $N = 8$  is shown to persist with large central charge and less spread of the neutron distribution in the surface region. With a low central charge and a large distribution of neutrons in the surface, we have therefore discussed the halo character of  $^{16}\text{C}$ ,  $^{19}\text{C}$ , and  $^{22}\text{C}$  nuclei in terms of their sharp increase in rms radii and extended densities.

- 
- [1] D. S. Ahn, N. Fukuda, H. Geissel, N. Inabe, N. Iwasa, T. Kubo, K. Kusaka, D. J. Morrissey, D. Murai, T. Nakamura, M. Ohtake, H. Otsu, H. Sato, B. M. Sherrill, Y. Shimizu, H. Suzuki, H. Takeda, O. B. Tarasov, H. Ueno, Y. Yanagisawa *et al.*, *Phys. Rev. Lett.* **123**, 212501 (2019).
- [2] I. Tanihata, H. Savajols, and R. Kanungo, *Prog. Part. Nucl. Phys.* **68**, 215 (2013).
- [3] D. Q. Fang, T. Yamaguchi, T. Zheng, A. Ozawa, M. Chiba, R. Kanungo, T. Kato, K. Morimoto, T. Ohnishi, T. Suda, Y. Yamaguchi, A. Yoshida, K. Yoshida, and I. Tanihata, *Phys. Rev. C* **69**, 034613 (2004).
- [4] I. Tanihata, H. Hamagaki, O. Hashimoto, Y. Shida, N. Yoshikawa, K. Sugimoto, O. Yamakawa, T. Kobayashi, N. Takahashi, *Phys. Rev. Lett.* **55**, 2676 (1985).
- [5] I. Tanihata, H. Hamagaki, O. Hashimoto, Y. Shida, N. Yoshikawa, K. Sugimoto, O. Yamakawa, T. Kobayashi, and N. Takahashi, *Phys. Lett. B* **289**, 261 (1992).
- [6] J. S. Al-Khalili and J. A. Tostevin, *Phys. Rev. C* **57**, 1846 (1998).
- [7] G. D. Alkhalzov, A. V. Dobrovolsky, P. Egelhof, H. Geissel, H. Irnich, A. V. Khanzadeev, G. A. Korolev, A. A. Lobodenko, G. Münzenberg, M. Mutterer, S. R. Neumaier, W. Schwab, D. M. Seliverstov, T. Suzuki, A. A. Vorobyov, *Nucl. Phys. A* **712**, 269 (2002).
- [8] G. A. Korolev, A. V. Dobrovolsky, A. G. Inglessi, G. D. Alkhalzov, P. Egelhof, A. Estradé, I. Dillmann, F. Farinon, H. Geissel, S. Ilieva, Y. Ke, A. V. Khanzadeev, O. A. Kiselev, J. Kurcewicz, X. C. Le, Yu. A. Litvinov, G. E. Petrov, A. Prochazka, C. Scheidenberger, L. O. Sergeev *et al.*, *Phys. Lett. B* **780**, 200 (2018).
- [9] S. Bagchi, R. Kanungo, W. Horiuchi, G. Hagen, T. D. Morris, S. R. Stroberg, T. Suzuki, F. Ameil, J. Atkinson, Y. Ayyad, D. Cortina-Gil, I. Dillmann, A. Estradé, A. Evdokimov, F. Farinon, H. Geissel, G. Guastalla, R. Janik, S. Kaur, R. Knöbel *et al.*, *Phys. Lett. B* **790**, 251 (2019).
- [10] K. J. Cook, T. Nakamura, Y. Kondo, K. Hagino, K. Ogata, A. T. Saito, N. L. Achouri, T. Aumann, H. Baba, F. Delaunay, Q. Deshayes, P. Doornenbal, N. Fukuda, J. Gibelin, J. W. Hwang, N. Inabe, T. Isobe, D. Kameda, D. Kanno, S. Kim *et al.*, *Phys. Rev. Lett.* **124**, 212503 (2020).
- [11] W. Horiuchi and Y. Suzuki, *Phys. Rev. C* **74**, 034311 (2006).
- [12] Y. Togano, T. Nakamura, Y. Kondo, J. A. Tostevin, A. T. Saito, J. Gibelin, N. A. Orr, N. L. Achouri, T. Aumann, H. Baba, F. Delaunay, P. Doornenbal, N. Fukuda, J. W. Hwang, N. Inabe, T. Isobe, D. Kameda, D. Kanno, S. Kim, N. Kobayashi *et al.*, *Phys. Lett. B* **761**, 412 (2016).
- [13] K. Tanaka, T. Yamaguchi, T. Suzuki, T. Ohtsubo, M. Fukuda, D. Nishimura, M. Takechi, K. Ogata, A. Ozawa, T. Izumikawa, T. Aiba, N. Aoi, H. Baba, Y. Hashizume, K. Inafuku, N. Iwasa, K. Kobayashi, M. Komuro, Y. Kondo, T. Kubo *et al.*, *Phys. Rev. Lett.* **104**, 062701 (2010).
- [14] N. Kobayashi, T. Nakamura, J. A. Tostevin, Y. Kondo, N. Aoi, H. Baba, S. Deguchi, J. Gibelin, M. Ishihara, Y. Kawada, T. Kubo, T. Motobayashi, T. Ohnishi, N. A. Orr, H. Otsu, H. Sakurai, Y. Satou, E. C. Simpson, T. Sumikama, H. Takeda *et al.*, *Phys. Rev. C* **86**, 054604 (2012).
- [15] D. Q. Fang, W. Q. Shen, J. Feng, X. Z. Cai, J. S. Wang, Q. M. Su, H. Y. Zhang, P. Y. Hu, Y. G. Ma, Y. T. Zhu, S. L. Li, H. Y. Wu, Q. B. Gou, G. M. Jin, W. L. Zhan, Z. Y. Guo, G. Q. Xiao, *Phys. Rev. C* **61**, 064311 (2000).
- [16] M. Rashdan, *Eur. Phys. J. A* **56**, 130 (2020).
- [17] R. Kanungo, W. Horiuchi, G. Hagen, G. R. Jansen, P. Navratil, F. Ameil, J. Atkinson, Y. Ayyad, D. Cortina-Gil, I. Dillmann, A. Estradé, A. Evdokimov, F. Farinon, H. Geissel, G. Guastalla, R. Janik, M. Kimura, R. Knobel, J. Kurcewicz, Yu. A. Litvinov *et al.*, *Phys. Rev. Lett.* **117**, 102501 (2016).
- [18] A. Ozawa, T. Kobayashi, T. Suzuki, K. Yoshida, and I. Tanihata, *Phys. Rev. Lett.* **84**, 5493 (2000).
- [19] A. Ozawa, T. Suzuki, and I. Tanihata, *Nucl. Phys. A* **693**, 32 (2001).
- [20] T. Zheng, T. Yamaguchi, A. Ozawa, M. Chiba, R. Kanungo, T. Kato, K. Katori, K. Morimoto, T. Ohnishi, T. Suda, I. Tanihata, Y. Yamaguchi, A. Yoshida, K. Yoshida, H. Toki, and N. Nakajima, *Nucl. Phys. A* **709**, 103 (2002).
- [21] R. J. Glauber, *Lectures in Theoretical Physics*, edited by W. E. Brittin (Interscience Publishers, New York, 1959), Vol. 1, p. 315.
- [22] Y. Ogawa, K. Yabana, and Y. Suzuki, *Nucl. Phys. A* **543**, 722 (1992).
- [23] S. Kox, A. Gamp, C. Perrin, J. Arvieux, R. Bertholet, J. F. Bruandet, M. Buenerd, R. Cherkaoui, A. J. Cole, Y. El-Masri, N. Longequeue, J. Menet, F. Merchez, and J. B. Viano, *Phys. Rev. C* **35**, 1678 (1987).



- [24] P. J. Karol, *Phys. Rev. C* **11**, 1203 (1975).
- [25] J. Chauvin, D. Lebrun, A. Lounis, and M. Buenerd, *Phys. Rev. C* **28**, 1970 (1983).
- [26] S. K. Charagi and S. K. Gupta, *Phys. Rev. C* **41**, 1610 (1990).
- [27] A. Ozawa, O. Bochkarev, L. Chulkov, D. Cortina, H. Geissel, M. Hellström, M. Ivanov, R. Janik, K. Kimura, T. Kobayashi, A. A. Korshennikov, G. Münzenberg, F. Nickel, Y. Ogawa, A. A. Ogloblin, M. Pfützner, V. Pribora, H. Simon, B. Sitár, P. Strmen *et al.*, *Nucl. Phys. A* **691**, 599 (2001).
- [28] H. Y. Zhang, W. Q. Shen, Z. Z. Ren, Y. G. Ma, W. Z. Jiang, Z. Y. Zhu, X. Z. Cai, D. Q. Fang, C. Zhong, L. P. Yu, Y. B. Wei, W. L. Zhan, Z. Y. Guo, G. Q. Xiao, J. S. Wang, J. C. Wang, Q. J. Wang, J. X. Li, M. Wang, and Z. Q. Chen, *Nucl. Phys. A* **707**, 303 (2002).
- [29] K. Makiguchi, W. Horiuchi, and A. Kohama, *Phys. Rev. C* **102**, 034614 (2020).
- [30] L. Ray, *Phys. Rev. C* **20**, 1857 (1979).
- [31] G. Giacornelli, *Progress in Nuclear Physics* (Pergamon, New York, 1970), Vol. 12.
- [32] D. J. Ernst, *Phys. Rev. C* **19**, 896 (1979).
- [33] L. C. Chamon, B. V. Carlson, L. R. Gasques, D. Pereira, C. De Conti, M. A. G. Alvarez, M. S. Hussein, M. A. Candido Ribeiro, E. S. Rossi, Jr., and C. P. Silva, *Phys. Rev. C* **66**, 014610 (2002).
- [34] Y. Matsuda, H. Sakaguchi, H. Takeda, S. Terashima, J. Zenihiro, T. Kobayashi, T. Murakami, Y. Iwao, T. Ichihara, T. Suda, T. Ohnishi, Y. Watanabe, H. Otsu, K. Yoneda, Y. Satou, K. Ozeki, and M. Kanazawa, *Phys. Rev. C* **87**, 034614 (2013).
- [35] I. Tanihata, T. Kobayashi, O. Yamakawa, S. Shimoura, K. Ekuni, K. Sugimoto, N. Takahashi, T. Shimoda, and H. Sato, *Phys. Lett. B* **206**, 592 (1988).
- [36] S. K. Charagi and S. K. Gupta, *Phys. Rev. C* **56**, 1171 (1997).
- [37] M. Y. H. Farag, *Czech. J. Phys.* **52**, 927 (2002).
- [38] L. A. Schaller, L. Schellenberg, T. Q. Phan, G. Piller, A. Ruetschi, and H. Schnewly, *Nucl. Phys. A* **379**, 523 (1982).
- [39] M. A. Hassanain, A. A. Ibraheem, and M. El-Azab Farid, *Phys. Rev. C* **77**, 034607 (2008).
- [40] S. Ahmad, A. A. Usmani, and Z. A. Khan, *Phys. Rev. C* **96**, 064602 (2017).
- [41] M. El-Azab Farid and G. R. Satchler, *Nucl. Phys. A* **438**, 525 (1985).
- [42] D. T. Khoa, *Phys. Rev. C* **63**, 034007 (2001).
- [43] M. Rashdan, *Phys. Rev. C* **86**, 044610 (2012).
- [44] I. Angeli, *At. Data Nucl. Data Tables* **87**, 185 (2004).
- [45] A. Shukla, B. K. Sharma, R. Chandra, P. Arumugam, and S. K. Patra, *Phys. Rev. C* **76**, 034601 (2007).
- [46] B. Abu-Ibrahim, W. Horiuchi, A. Kohama, and Y. Suzuki, *Phys. Rev. C* **77**, 034607 (2008).
- [47] A. Ozawa, I. Tanihata, T. Kobayashi, Y. Sugahara, O. Yamakawa, K. Omata, K. Sugimoto, D. Olson, W. Christie, and H. Wieman, *Nucl. Phys. A* **608**, 63 (1996).
- [48] A. Ozawa, D. Q. Fang, M. Fukuda, N. Iwasa, T. Izumikawa, H. Jeppesen, R. Kanungo, R. Koyama, T. Ohnishi, T. Ohtsubo, W. Shinozaki, T. Suda, T. Suzuki, M. Takahashi, I. Tanihata, C. Wu, and Y. Yamaguchi, *Phys. Rev. C* **78**, 054313 (2008).
- [49] C. Wu, Y. Yamaguchi, A. Ozawa, R. Kanungo, I. Tanihata, T. Suzuki, D. Q. Fang, T. Suda, T. Ohnishi, M. Fukuda, N. Iwasa, T. Ohtsubo, T. Izumikawa, R. Koyama, W. Shinozaki, and M. Takahashi, *Nucl. Phys. A* **739**, 3 (2004).
- [50] M. Fukuda, T. Ichihara, N. Inabe, T. Kubo, H. Kumagai, T. Nakagawa, Y. Yano, I. Tanihata, M. Adachi, K. Asahi, M. Kouguchi, M. Ishihara, H. Sagawa, and S. Shimoura, *Phys. Lett. B* **268**, 339 (1991).
- [51] A. Khouaja, A. C. C. Villari, M. Benjelloun, D. Hirata, G. Auger, H. Savajols, W. Mittig, P. Roussel-Chomaz, N. A. Orr, M. G. Saint-Laurent, S. Pita, A. Gillibert, M. Chartier, C. E. Demonchy, L. Giot, D. Baiborodin, Y. Penionzhkevich, W. N. Catford, A. Lépine-Szily, and Z. Dlouhy, *Nucl. Phys. A* **780**, 1 (2006).
- [52] A. Khouaja, A. C. C. Villari, M. Benjelloun, G. Auger, D. Baiborodin, W. Catford, M. Chartier, C. E. Demonchy, Z. Dlouhy, A. Gillibert, L. Giot, D. Hirata, A. LépineSzily, W. Mittig, N. Orr, Y. Penionzhkevich, S. Pita, P. Roussel-Chomaz, M. G. Saint-Laurent, and H. Savajols, *Eur. Phys. J. A* **25**, 223 (2005).
- [53] T. Yamaguchi, I. Hachiuma, A. Kitagawa, K. Namihira, S. Sato, T. Suzuki, I. Tanihata, and M. Fukuda, *Phys. Rev. Lett.* **107**, 032502 (2011).
- [54] G. F. Bertsch, B. A. Brown, and H. Sagawa, *Phys. Rev. C* **39**, 1154 (1989).
- [55] I. Tanihata, S. Terashima, R. Kanungo, F. Ameil, J. Atkinson, Y. Ayyad, D. Cortina-Gil, I. Dillmann, A. Estradé, A. Evdokimov, F. Farinon, H. Geissel, G. Guastalla, R. Janik, R. Knoebel, J. Kurcewicz, Yu. A. Litvinov, M. Marta, M. Mostazo, I. Mukha *et al.*, *Prog. Theor. Exp. Phys.* **2016**, 043D05 (2016).
- [56] D. T. Tran, H. J. Ong, T. T. Nguyen, I. Tanihata, N. Aoi, Y. Ayyad, P. Y. Chan, M. Fukuda, T. Hashimoto, T. H. Hoang, E. Ideguchi, A. Inoue, T. Kawabata, L. H. Khiem, W. P. Lin, K. Matsuta, M. Mihara, S. Momota, D. Nagae, N. D. Nguyen *et al.*, *Phys. Rev. C* **94**, 064604 (2016).
- [57] D. T. Tran, H. J. Ong, G. Hagen, T. D. Morris, N. Aoi, T. Suzuki, Y. Kanada-Enyo, L. S. Geng, S. Terashima, I. Tanihata, T. T. Nguyen, Y. Ayyad, P. Y. Chan, M. Fukuda, H. Geissel, M. N. Harakeh, T. Hashimoto, T. H. Hoang, E. Ideguchi, A. Inoue *et al.*, *Nat. Commun.* **9**, 1594 (2018).
- [58] Y. Suzuki, W. Horiuchi, S. Terashima, R. Kanungo, F. Ameil, J. Atkinson, Y. Ayyad, D. Cortina-Gil, I. Dillmann, A. Estradé, A. Evdokimov, F. Farinon, H. Geissel, G. Guastalla, R. Janik, R. Knoebel, J. Kurcewicz, Yu. A. Litvinov, M. Marta, M. Mostazo *et al.*, *Phys. Rev. C* **94**, 011602(R) (2016).
- [59] G. Audi, O. Bersillon, J. Blachot, and A. H. Wapstra, *Nucl. Phys. A* **624**, 1 (1997).
- [60] T. Nakamura, N. Fukuda, T. Kobayashi, N. Aoi, H. Iwasaki, T. Kubo, A. Mengoni, M. Notani, H. Otsu, H. Sakurai, S. Shimoura, T. Teranishi, Y. X. Watanabe, K. Yoneda, and M. Ishihara, *Phys. Rev. Lett.* **83**, 1112 (1999).